

CMB constraints on light dark matter candidates

C. Evoli^{1*}, S. Pandolfi² and A. Ferrara³

¹ *II. Institut für Theoretische Physik, Universität Hamburg, Luruper Chaussee 149, D-22761 Hamburg, Germany*

² *Dark Cosmology Centre, Niels Bohr Institute, University of Copenhagen, Juliane Maries Vej 30, DK-2100 Copenhagen, Denmark*

³ *Scuola Normale Superiore, Piazza dei Cavalieri 7, 56126 Pisa, Italy*

26 October 2012

ABSTRACT

Unveiling the nature of cosmic dark matter is an urgent issue in cosmology. Here we make use of a strategy based on the search for the imprints left on the CMB temperature and polarization spectra by the energy deposition due to annihilations of the most promising dark matter candidate, a stable WIMP of mass $m_\chi = 1 - 20$ GeV. A major improvement with respect to previous similar studies is a detailed treatment of the annihilation cascade and its energy deposition in the cosmic gas. This is vital as this quantity is degenerate with the annihilation cross-section $\langle\sigma v\rangle$. The strongest constraints are obtained from Monte Carlo Markov Chains analysis of the combined WMAP7 and SPT datasets up to $\ell_{\max} = 3100$. If annihilation occurs via the $e^+ - e^-$ channel, a light WIMP can be excluded at $2\text{-}\sigma$ c.l. as a viable DM candidate in the above mass range. However, if annihilation occurs via $\mu^+ - \mu^-$ or $\tau^+ - \tau^-$ channels instead we find that WIMPs with $m_\chi > 5$ GeV might represent a viable cosmological DM candidate.

We compare the results obtained in the present work with those obtained adopting an analytical simplified model for the energy deposition process widely used in literature, and we found that realistic energy deposition descriptions can influence the resulting constraints up to 60%.

Key words: dark matter

1 INTRODUCTION

According to the widely accepted Lambda Cold Dark Matter (Λ CDM) cosmology, the Universe is mostly made of *dark* components, i.e. Dark Energy (75% of the mass-energy budget) and Dark Matter (DM, 20%); these components largely dominate over baryons (Komatsu et al. 2011). The situation is then rather unsatisfactory as the nature of the dark components is far from being established and it stands as one of the most crucial issues in cosmology.

The most promising DM interpretation is in terms of a thermal relic density of stable weakly interacting massive particles (WIMPs). An appealing feature of such a scenario is that the annihilation cross-sections predicted by the electroweak scale automatically provide the right DM density after freeze-out (Bertone & Silk 2010). This argument applies equally well to particles with $1 - 20$ GeV masses as to those with masses more traditionally associated with supersymmetric neutralinos ($m_\chi \sim 40 - 1000$ GeV).

In the recent years, evidences have been accumulating in favor of DM in the form of ~ 10 GeV WIMPs. In fact,

a relatively light DM particle with an annihilation cross-section consistent with that predicted for a simple thermal relic ($\langle\sigma v\rangle_T \sim 10^{-26} \text{ cm}^3 \text{ s}^{-1}$) and a distribution in the halo of the Milky Way consistent with that predicted from simulations could accommodate the indirect detection of gamma rays from the Galactic Center, the synchrotron emission from the Milky Way radio filaments and the diffuse synchrotron emission from the Inner Galaxy (the so-called “WMAP Haze”) (Hooper, Finkbeiner & Dobler 2007; Hooper & Linden 2011a,b; Dobler et al. 2010; Finkbeiner 2004).

At the same time it would be compatible with claims of low-energy signals from DM direct detection experiments as DAMA/LIBRA, CoGeNT, and CRESST-II. In particular, the striking detection of annual modulation observed by DAMA/LIBRA (now supported by CoGeNT) is hardly consistent with all known standard backgrounds. Notice, however, that (a) other experiments, as Xenon100, have not confirmed the result of the direct detections, and (b) indirect detection features might have alternative astrophysical explanations (Bernabei et al. 2008; Biermann et al. 2010; Akerib et al. 2010; CDMS II Collaboration et al. 2010; Bernabei et al.

* E-mail: carmelo.evoli@desy.de

2010; Crocker & Aharonian 2011; Aalseth et al. 2011a,b; Aprile et al. 2011; XENON100 Collaboration et al. 2012; Guo & Mathews 2012).

A phenomenological model of light DM particle able to accommodate the collection of indirect and direct observations should require that DM annihilates primarily into leptons with a cross-section close to $\langle\sigma v\rangle_T$. Moreover, approximately 20% of annihilations must also proceed to hadronic final states in order to yield a spin-independent, elastic scattering cross-section ($\approx 10^{-41}$ cm²) with nucleons compatible with the direct detection (see Hooper 2012, for a detailed review).

The light DM hypothesis implies a larger cosmic number density of such particles ($n_{\text{DM}} \propto \Omega_{\text{DM}} h^2 / m_{\text{DM}}$); in addition, the annihilation rate ($\propto n_{\text{DM}}^2 \propto (1+z)^6$) increases dramatically at early cosmic times. These two facts imply that the annihilation energy deposition might profoundly affect the thermal and ionization history of the Intergalactic Medium (IGM)¹ prior to reionization. In turn, this modified evolution with respect to the standard recombination scenario can in principle leave detectable signatures on the CMB spectrum². Determining the amplitude of this effect is the chief goal of the present study.

The effects of the DM annihilation around the redshift of the last scattering surface (LSS) have been discussed in Slatyer, Padmanabhan & Finkbeiner (2009) and are only briefly summarized here. The extra free-electrons resulting from the DM energy cascade scatter CMB photons, thus thickening the LSS and in principle shifting the position of the peaks in the temperature-temperature (TT) power spectrum. In practice, reasonable electron density excesses yield corrections to the positions of the peaks that can be safely ignored here. More importantly, oscillations on scales smaller than the LSS width are damped in the TT and EE spectra in a manner inversely proportional to their wavelength. Such DM annihilation effects on the TT spectrum are degenerate with variations of the slope (n_s) and amplitude (A_s) of the primordial power spectrum, and, to a lesser extent, with the baryon ($\Omega_b h^2$) and DM ($\Omega_{\text{DM}} h^2$) density parameter. Polarization spectra are generated via Thomson scattering of the local quadrupole in the temperature distribution. As the broadening of the last scattering surface increases the intensity of the quadrupole moment, the EE spectrum is enhanced on large scales. Furthermore, it can be shown (i.e. Padmanabhan & Finkbeiner 2005) that the quadrupole is dominated by the free-streaming from the dipole perturbation that is $\pi/2$ out of phase of the monopole. A thicker LSS boosts the fractional contribution from the monopole, thus slightly shifting the peaks of the EE and TE spectra.

A key aspect of these calculations is that only a fraction of the released energy is finally deposited into the IGM in the form of heating and H/He ionizations. However, earlier studies (Padmanabhan & Finkbeiner 2005; Mapelli, Ferrara & Pierpaoli 2006; Galli et al. 2009) have used a simplified description of such processes, based

on the hypothesis that a redshift-independent fraction of the DM rest-mass energy is absorbed by the IGM. More recently (Slatyer, Padmanabhan & Finkbeiner 2009; Galli et al. 2011; Hütsi et al. 2011) have reassessed the energy deposition problem including various energy-loss mechanisms in a more realistic way. This approach, based on semi-analytical solutions lacks an implementation of low-energy atomic processes that determine the actual absorption channel (e.g. heating, ionization, excitations) and because of this they have to rely on the results of Chen & Kamionkowski (2004). To fill this gap here we build upon our previous work (Valdés, Evoli & Ferrara 2010) in which we developed the MEDEA (Monte Carlo Energy Deposition Analysis) code which includes Bremsstrahlung and inverse Compton processes, along with H/He collisional ionizations and excitations, and electron-electron collisions. MEDEA enables us to compute the energy partition into heating, excitations and ionizations as a function of the primary initial energy, the gas ionization fraction and the redshift. MEDEA has been recently improved (Evoli et al. 2012) to include the energy cascade from particles generated by primary leptons/photons using the most up-to-date cross-sections and extending the validity of the model to unprecedented high (\sim TeV) energies (see Shull 1979; Shull & van Steenberg 1985; Furlanetto & Stoeveit 2010). In addition, arbitrary initial energy distribution of electrons, positrons and photons can be assigned. These improvements make MEDEA suitable for studying the IGM energy deposition for some of the most popular DM candidates (Evoli et al. 2012). With this greatly improved physical description we aim at computing the signatures left in the CMB spectrum by annihilating light DM.

2 METHOD

In this Section we compute the energy input of DM annihilations in the IGM. This approach is similar in spirit to a number of recent works (Padmanabhan & Finkbeiner 2005; Galli et al. 2009; Hütsi, Hektor & Raidal 2009; Slatyer, Padmanabhan & Finkbeiner 2009; Galli et al. 2011; Hütsi et al. 2011); however, we improve upon them by a more accurate description of the energy deposition channels.

2.1 Modified ionization history

For the reasons given in the Introduction, we concentrate on light DM candidates that annihilate mainly in leptonic channels. In Fig. 1 we show the annihilation spectra of a 10 GeV DM particle for the different annihilation channels, computed using the public code DarkSUSY. The muonic and tauonic channels produce a leptonic pair whose prompt annihilation gives rise to an energy spectrum of primary electrons or positrons with kinetic energy from 10 GeV down to few tens of MeV; annihilation in the electron channel produces a electron/positron pair in which both the two primary leptons have a kinetic energy which is the mass of the annihilation particle.

The total energy density input from DM annihilations

¹ Strictly speaking, the term “Intergalactic Medium” is ill-defined before the epoch of galaxy formation. Nevertheless, following common practice, we will use it anyway.

² Leptons and photons deposit their energy very efficiently in the IGM; hence leptonic channels are expected to leave a stronger CMB signature

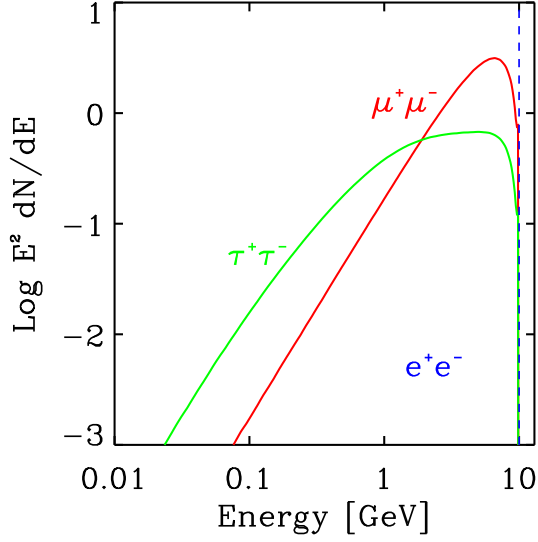


Figure 1. Energy spectrum of electrons or positrons from the annihilation of a 10 GeV mass WIMP into e^+e^- , $\mu^+\mu^-$ and $\tau^+\tau^-$ channels.

is:

$$\begin{aligned} \frac{dE_{\text{DM}}}{dt}(z) &= \rho_c^2 c^2 \Omega_{\text{DM}}^2 (1+z)^6 \frac{\langle \sigma v \rangle}{m_{\text{DM}}} \\ &\approx 4.03 \times 10^{-38} \left(\frac{\Omega_{\text{DM}} h^2}{0.11} \right) (1+z)^6 B \left(\frac{m_{\text{DM}} c^2}{\text{GeV}} \right)^{-1} \text{ GeV cm}^{-3} \text{ s}^{-1} \end{aligned} \quad (1)$$

where $\rho_c = 3H_0^2/8\pi G$ is the critical density of the universe today, Ω_{DM} is the DM density contribution to the critical density, m_{DM} is the mass of the DM particle and $\langle \sigma v \rangle$ is the thermally averaged product of the cross-section and relative velocity of the annihilating DM particles. Moreover we have defined $B \equiv \langle \sigma v \rangle / 3 \times 10^{-26} \text{ cm}^3 \text{ s}^{-1}$. Notice that eq. 1 is valid only for DM Majorana particles.

In the light of the earlier works of [Cirelli, Iocco & Panci \(2009\)](#) and [Hütsi et al. \(2011\)](#) we neglect the role of structure formation in the calculation of the energy deposition. In fact, halos with density higher than the background could in principle boost the average annihilation rate, however their formation starts at a relative low-redshift ($z \lesssim 100$) when the ionization rate due to DM annihilation is already negligible.

By introducing the mean number density of hydrogen nuclei $n_{\text{H}} \approx 1.9 \times 10^{-7} (1+z)^3 \text{ cm}^{-3}$, and the parameter

$$\epsilon_0 \equiv 2.12 \times 10^{-31} \left(\frac{\Omega_{\text{DM}} h^2}{0.11} \right) B \left(\frac{m_{\text{DM}} c^2}{\text{GeV}} \right)^{-1}, \quad (2)$$

eq. 1 becomes:

$$\frac{dE_{\text{DM}}}{dt}(z) = \epsilon_0 n_{\text{H}} (1+z)^3 \text{ GeV s}^{-1} \quad (3)$$

It has been pointed out that $\langle \sigma v \rangle$ could be somewhat boosted by the Sommerfeld effect (e.g. [Galli et al. 2009](#); [Slatyer, Padmanabhan & Finkbeiner 2009](#)). Although it is easy to implement this process in this scheme we have not

considered here as it depends strongly on the DM model chosen ([van den Aarsen, Bringmann & Goedecke 2012](#)).

To derive the DM-modified cosmic ionization/thermal history, we need to include the above heating (and corresponding ionization) rate into the relevant detailed balance equations. To this aim we have modified that publicly available code³ [RECFAST](#) ([Seager, Sasselov & Scott 1999](#)), part of the [CAMB](#) ([Lewis, Challinor & Lasenby 2000](#)) code, by adding the following terms:

$$-\frac{dx_{\text{H}}}{dz} = \frac{1}{H(z)(1+z)} f_{\text{ion,H}}(z) \frac{dE_{\text{DM}}/dt}{n_{\text{H}}(z)E_{\text{ion,H}}} \quad (4)$$

$$-\frac{dx_{\text{He}}}{dz} = \frac{1}{H(z)(1+z)} f_{\text{ion,He}}(z) \frac{dE_{\text{DM}}/dt}{n_{\text{H}}(z)E_{\text{ion,He}}} \quad (5)$$

$$-\frac{dT_{\text{M}}}{dz} = \frac{1}{H(z)(1+z)} \frac{2}{3k_{\text{B}}} \frac{f_{\text{h}}(z)}{1+f_{\text{He}}+x_{\text{e}}(z)} \frac{dE_{\text{DM}}/dt}{n_{\text{H}}(z)} \quad (6)$$

where $f_{\text{ion,H}}$, $f_{\text{ion,He}}$ (f_{h}) are energy deposition fractions into H or He ionizations (heating) including those induced by Ly α photons on atoms in the excited states.

A key point to take from eqs. 4–6 is that energy deposition fractions are fully degenerate with the parameter we aim to constrain, i.e. $\langle \sigma v \rangle$. To partly alleviate this difficulty, a possible strategy, first proposed by [Ripamonti et al. 2005](#), is to determine the lowest possible bound by assuming $f_{\text{h}} = f_{\text{ion}} = 1$. More often, constraints have been derived by using the [Chen & Kamionkowski \(2004\)](#) prescription for f_{i} . Based on the results of [Shull & van Steenberg \(1985\)](#), these authors pointed out that when the gas is mostly neutral, energy is evenly distributed among ionizations, excitation and heating; for a fully ionized medium, almost all of the energy goes instead into gas heating. A linear interpolation is used for intermediate ionization values:

$$f_{\text{i}} = \frac{1}{3}(1 - x_{\text{e}}) \quad (7)$$

$$f_{\text{h}} = \frac{1}{3}(1 + 2x_{\text{e}}) \quad (8)$$

This approximation is too crude to be used for high-precision predictions as clearly shown by the comparison with fully-fledged Monte Carlo simulations ([Valdés et al. 2007](#); [Furlanetto & Stoever 2010](#)). Moreover, for primary energies $\gtrsim 1$ MeV inverse Compton energy losses on the CMB becomes important and introduce a significant redshift dependence of the fractions. These processes have been carefully modeled in [Evoli et al. \(2012\)](#) and here we use their results for f_{i} . Note that the latter assume that photon energy deposition occurs locally, which is not true in general (see [Slatyer, Padmanabhan & Finkbeiner 2009](#)). In Appendix A we show that this approximation is very accurate in the energy range of interest here. The energy depositions calculated with MEDEA are shown in Fig. 2 for different annihilation channels of a 10 GeV DM particle mass. Such curves show a dependence on the annihilation channel since different initial spectral distributions involve different energy loss mechanisms. For computational speed-up purposes we have

³ Recently other similar codes (e.g. CosmoREC, HyREC) have improved the precision of the results implementing a more detailed description of the atomic structure ([Hütsi et al. 2011](#); [Giesen et al. 2012](#)). However, given the current precision of CMB experiments, these corrections do not affect our conclusions.

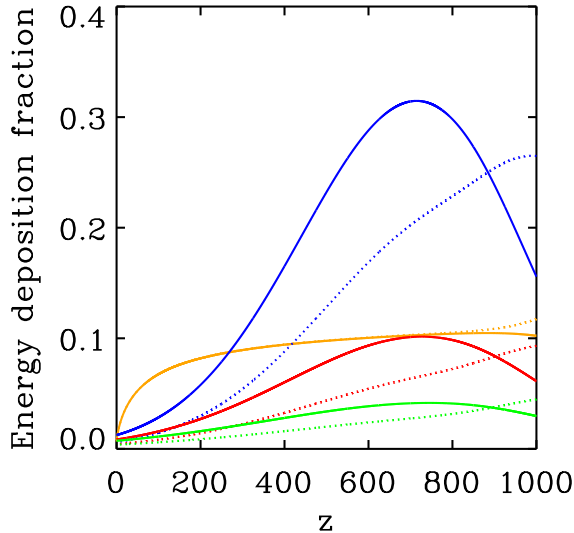


Figure 2. Fractional energy depositions into H and He ionization (solid lines) and heating (dotted lines) from DM annihilation of a 10 GeV DM candidate as function of redshift. Color code as in Fig. 1. The orange lines show the energy deposition fractions obtained from the simplified deposition model described in Sec. 3.1 for annihilation into muons. In this plot we assume the standard IGM ionization evolution based on a WMAP7 cosmology.

derived handy fitting formulae, given in Appendix B, to the MEDEA numerical results.

2.2 MCMC analysis

To obtain a constraint on the annihilation cross-section of light DM candidate, we have performed a Monte Carlo Markov Chains (MCMC) analysis using publicly available CosmoMC package (Lewis & Bridle 2002). We consider here a flat Λ CDM model with the canonical six parameters plus an additional seventh one, $\langle\sigma v\rangle$. Therefore the theoretical model we adopt is described by the following set of parameters:

$$\{\omega_b, \omega_{\text{DM}}, \theta_s, \tau, n_s, \log[10^{10} A_s], \langle\sigma v\rangle\}, \quad (9)$$

where $\omega_b \equiv \Omega_b h^2$, $\omega_{\text{DM}} \equiv \Omega_{\text{DM}} h^2$ are the baryons and cold dark matter density parameters, θ_s is the ratio between the sound horizon and the angular diameter distance at decoupling, τ is the optical depth, n_s is the scalar spectral index, A_s is the amplitude of the primordial spectrum. The flat priors assumed for these parameters are shown in Tab. 1.

Our basic data set is the seven-year WMAP temperature and polarization data (Komatsu et al. 2011; Larson et al. 2011). We consider purely adiabatic initial conditions and we impose spatial flatness. We also fixed the primordial fractional abundance of Helium to the standard observed nominal value of $Y_{\text{He}} = 0.24$. We refer to this basic dataset as “WMAP7”. For each case we run 5 chains; convergence diagnostic tests are performed using the Gelman and Rubin “variance of chain mean/mean of chain variances” R-1 statistics. We consider the chains to be converged only if $R - 1 < 0.03$. The 68% and 95% confidence level

Parameter	Prior
$\Omega_b h^2$	0.005-0.1
$\Omega_{\text{DM}} h^2$	0.01-0.99
θ_s	0.5-10
τ	0.01-0.8
n_s	0.5-1.5
$\ln(10^{10} A_s)$	2.7-4
$\langle\sigma v\rangle/\text{cm}^3 \text{ s}^{-1}$	$0 - 10^{-24}$

Table 1. Adopted flat priors for the cosmological parameters.

(c.l.) one- and two-dimensional constraints are obtained after marginalization over the remaining “nuisance” parameters. We have tested that varying H_0 instead of θ_s , as suggested in Galli et al. (2009), our results are affected by less than 5%.

In addition to the WMAP7 dataset we also consider the case “CMB ALL+SPT”. In this larger dataset we include, in addition to the WMAP data, the CMB temperature and polarization data from QUaD (Brown et al. 2009), and the recent SPT (Keisler et al. 2011) data. The inclusion of the QUaD experiment (a) enlarges the multipole range considered for the temperature, allowing to probe the small-scale region $500 \leq \ell \leq 2500$, and (b) adds information on the E - and B -mode polarization. Moreover, the SPT experiment pushes the dynamic range of CMB observations to larger multipoles with the respect of WMAP7, measuring with a better accuracy the damping tail of the CMB angular power spectrum. We consider data up to $\ell = 3100$. For the SPT experiment it is necessary to account for foreground contributions by adding three extra parameters representing the amplitude of the SZ, A_{SZ} , clustering, A_C , and shot-noise, A_P , signal from point sources. We used for each foreground component the proper template provided by (Keisler et al. 2011). When deriving our constraints we marginalize over these three nuisance parameters. To compute the likelihood of the data we have properly modified the CosmoMC package in order to make use of the routine supplied by the WMAP team for the WMAP7 dataset, publicly available at the LAMBDA website⁴, and of the likelihood code provided by the SPT team (Keisler et al. 2011) for the SPT experiment.

As we already discussed in the introduction the inclusion of small scale CMB measurements can greatly help in breaking the degeneracy with the other cosmological parameters, and in particular with n_s , thus improving the constraints on the DM sector parameters. Moreover, the addition of the SPT data to the WMAP data improves the constraints on the ratio of the sound horizon to the angular diameter distance parameter θ_s by nearly a factor of two (Keisler et al. 2011), thus narrowing the allowed range of the other parameters.

We adopt the standard parametrization for the reionization, considered as an instantaneous process occurring at some redshift z_r , with $z_r < 32$. Such choice leads to a one-to-one relation between z_r and the adopted e.s. optical depth τ . As a caveat, we note that Pandolfi et al. (2011)

⁴ <http://lambda.gsfc.nasa.gov/>

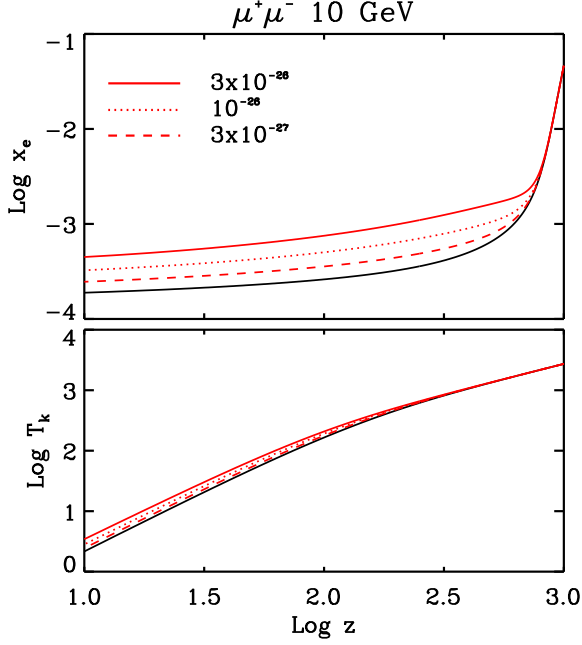


Figure 3. DM-modified ionization (top) and thermal (bottom) histories for a 10 GeV WIMP annihilating into muons. Values of the annihilation cross-section correspond to different curves as shown by the legend. The black solid line represents the case case without DM annihilations.

showed that a more realistic reionization modeling might affect the cosmological parameters that are more degenerate with the DM annihilation cross-section, thus introducing an additional source of uncertainty.

3 RESULTS

DM-modified ionization and thermal histories for a 10 GeV WIMP annihilating into muons on top of a Λ CDM model are shown in Fig. 3; the corresponding TT (EE) spectrum is shown in Fig. 4 (Fig. 5). Qualitatively similar conclusions can be drawn for the other channels. The energy released in form of electrons and positrons from the annihilation of DM particles delays and quenches the recombination processes, thus resulting in a freeze-out relic electron fraction a factor of a few larger, depending on the value of $\langle\sigma v\rangle$. For the same reason, the temperature drop with time is less pronounced. As a consequence of the higher ionization rate, the CMB normalization value is smaller.

We follow the procedure described in Sec. 2.2 to get constraints on the cosmological parameters in (9) and we compare them with those obtained by the WMAP team from their 7-yr data. We present in Fig. 6 the 2-sigma c.l. constraints on the DM annihilation cross-section $\langle\sigma v\rangle$ as function of the DM mass. Differently to (e.g. Galli et al. 2009) our results cannot be given as a single number due to the mass dependence of the energy deposition fractions (see Sec. 2.1). A detailed comparison with their results will be given in Section 3.1. The main conclusion is that only DM candidates lighter than $\lesssim 10$ GeV annihilating via the $e^+ - e^-$ channel can be excluded as a dominant component of the DM energy-density. The constraints are stronger, as

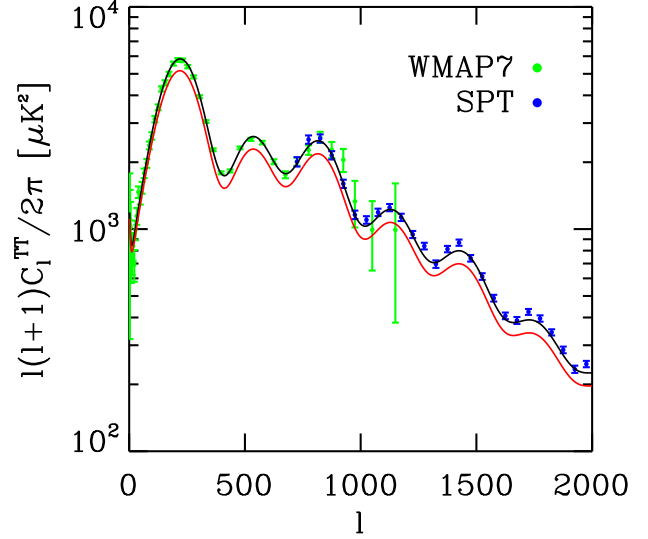


Figure 4. Angular power spectrum of CMB temperature fluctuations: standard case without DM annihilations (black line), considering the $\mu^+ - \mu^+$ a 10 GeV WIMP with $\langle\sigma v\rangle = 3 \times 10^{-26} \text{ cm}^3 \text{ s}^{-1}$ (red line). The points with errorbars show the 7-year measurements of the WMAP satellite (black) and the SPT data (blue).

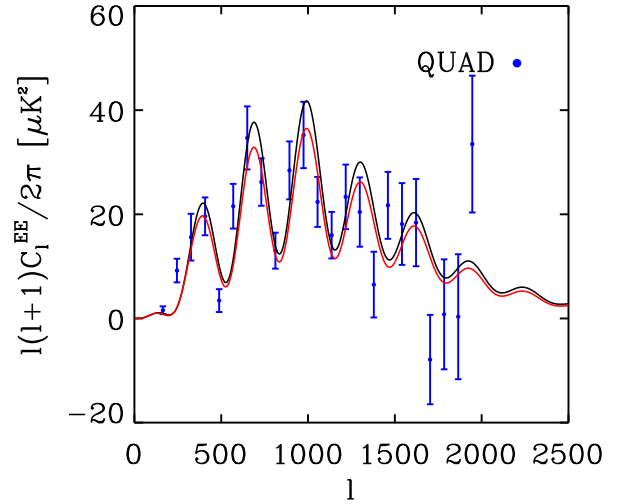


Figure 5. As in Fig. 4 for the polarization fluctuations. The points with error bars show the measurements of the QUAD experiment.

expected, if we include in the present analysis the recent SPT dataset with $\ell_{\text{max}} = 3100$ ⁵ and the polarization data. In this case the electron channel is excluded in the entire mass range (up to 20 GeV), where the other two channels can be excluded for masses $\lesssim 5$ GeV.

⁵ We have verified that our results are insensitive for choice of $3000 \lesssim \ell_{\text{max}} \lesssim 3500$.

We have verified that the stronger constraints come mainly from the SPT data inclusion, since the polarization data alone improve the constraints by $< 3\%$. Currently polarization data alone are not of sufficient quality to robustly constrain DM parameters. Future experiments, specifically devoted to measure polarization at smaller scales like Planck (Tauber et al. 2010), PolarBear (Anthony 2012) and CMBPol (Zaldarriaga et al. 2008) are expected to significantly improve the situation.

The CMB constraints we find are weaker than the constraints obtained by the FERMI experiment using the signal in the diffuse isotropic gamma emission from the Galaxy (Abdo et al. 2010) and from a combined analysis of the Milky Way satellites Ackermann et al. (2011); Baushev, Federici & Pohl (2012); Cholis & Salucci (2012). Comparing the 10 GeV case of annihilation channel in muons and taus, the inferred maximum cross-section from FERMI falls below the thermal value. However, in their analysis the rather uncertain distribution of DM in galaxies must be specified, while the present approach is free from any such hypothesis.

In Table 3 we report the 68% c.l. constraints on the cosmological parameters for the 10 GeV muon annihilation channel for the *WMAP7*, *CMB ALL+SPT* cases, and the *WMAP7* alone dataset, i.e. a minimal Λ CDM model without annihilating DM (“*WMAP7* (Standard)”). The one-dimensional posterior probability for $\Omega_b h^2$, $\Omega_{\text{DM}} h^2$ and n_s , for the three dataset cases considered is also shown in Fig. 7. The strongest shift occurs for the baryon density $\Omega_b h^2$ which in the minimal, 6-parameter, standard case is $\Omega_b h^2 = 0.0226 \pm 0.0006$, whereas, after the inclusion of the annihilating DM, becomes $\Omega_b h^2 = 0.0224 \pm 0.0006$ in the case of *WMAP7*, and $\Omega_b h^2 = 0.0217 \pm 0.0004$ in the case of *CMB ALL+SPT*. This lower baryon density required results from the increased number of electrons produced DM annihilations; the two factors combine to give the same optical final depth needed to match the CMB data. The constraints on the dark matter density are only barely affected by the introduction of the DM annihilation, while instead the constraints on the scalar spectral index of primordial perturbations are shifted to higher values. Similarly to the case of $\Omega_b h^2$, but in the opposite direction, the extra energy injected by the DM annihilation leads to a damping of the tail of CMB power spectrum, so that n_s has to be increased in order to compensate for this effect and still provide a good fit to the data. Notice that in the case of *WMAP7*, the introduction of DM annihilation makes the Harrison-Zel’dovich value for the scalar spectral index $n_s = 1$ compatible with the data within two standard deviations, while instead when also the SPT dataset is added the scale invariant power spectrum is again ruled out by the data.

3.1 Simplified energy deposition model

As we have stressed already, using a correct description of the energy deposition fractions is crucial to derive reliable DM constraints. Here we intend to quantify this statement by comparing our results with the constraints obtained using an approximated energy deposition model.

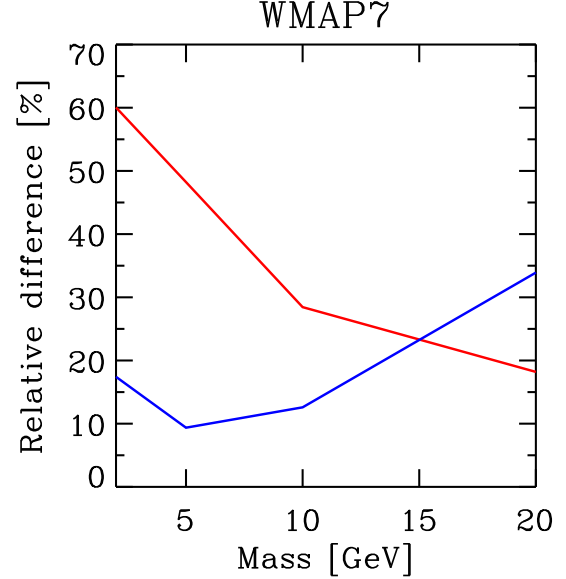


Figure 8. Relative differences [(MEDEA-simplified)/MEDEA] between the constraints obtained with a simple energy deposition model as described in Sec. 3.1 and using the energy deposition fractions obtained with the MEDEA code. Color code as in Fig. 1

This is summarized by the following expressions:

$$f_{\text{ion,H}} = \tilde{C}_H \frac{1 - x_e}{3} = \tilde{C}_H \frac{1 + 2f_{\text{He}} - x}{3(1 + 2f_{\text{He}})} \quad (10)$$

$$f_{\text{ion,He}} = \tilde{C}_{\text{He}} \frac{1 - x_e}{3} = \tilde{C}_{\text{He}} \frac{1 + 2f_{\text{He}} - x}{3(1 + 2f_{\text{He}})} \quad (11)$$

$$f_h = \frac{1 + 2x_e}{3} = \frac{(1 + 2f_{\text{He}}) + 2x}{3(1 + 2f_{\text{He}})} \quad (12)$$

where $x \equiv x_H + f_{\text{He}} x_{\text{He}}$ is a convenient variable to be used in RECFAST and

$$\tilde{C}_H = C_H + (1 - C_H) \frac{E_{\text{ion,H}}}{E_{\alpha,\text{H}}} \quad (13)$$

(a similar expression is valid for the He) where C_H and C_{He} are the Peebles factors as given in Wong, Moss & Scott (2008). As in Galli et al. (2011) we have multiplied these formulas for the $f_{\text{abs}}(z)$ given by Slatyer, Padmanabhan & Finkbeiner (2009) for the DM annihilation in electrons or muons at 1 GeV.

In Fig. 2 we show the corresponding energy depositions as function of redshift for the muon channel and we compare with what obtained from the Monte Carlo simulations. It is evident that this simplified approach over predicts the energy deposition for almost the entire redshift range.

We have verified that using the analytic expression in eq.s 10–12 the derived constraints at 1 GeV are coincident with the results reported in Tab. II by Galli et al. (2011) either for the muon and the electron channel.

In Fig. 8 we show the relative differences between our results and the results obtained adopting the simplified model. We compare the case in which only *WMAP7* data are used. In the range $m_{\text{DM}} = 1 - 20$ GeV the differences can be quoted between 10% and 30% for the electron channel, and between 20% and 60% for the muon channel. The constraints we get always tend to be weaker than those given

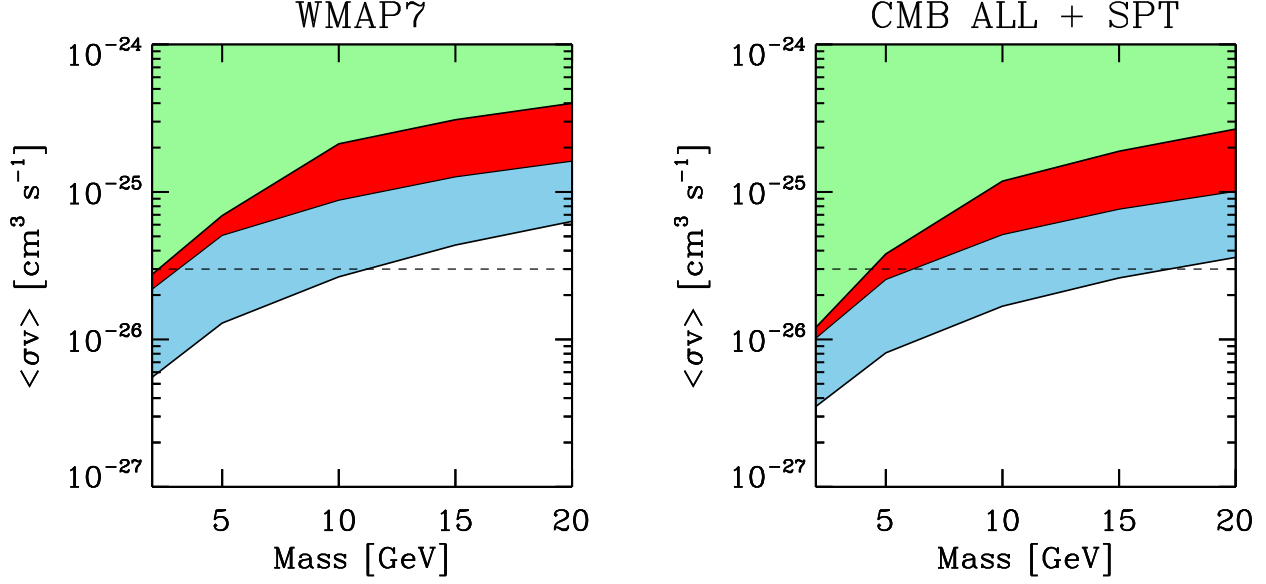


Figure 6. Constraint plot on the maximum cross-section for different DM candidates based on *WMAP7* and *CMB ALL+SPT* dataset (the region excluded for the tau annihilation channel is indicated in green, while the additional region excluded for the muon (electron) annihilation channel is indicated in red (blue)).

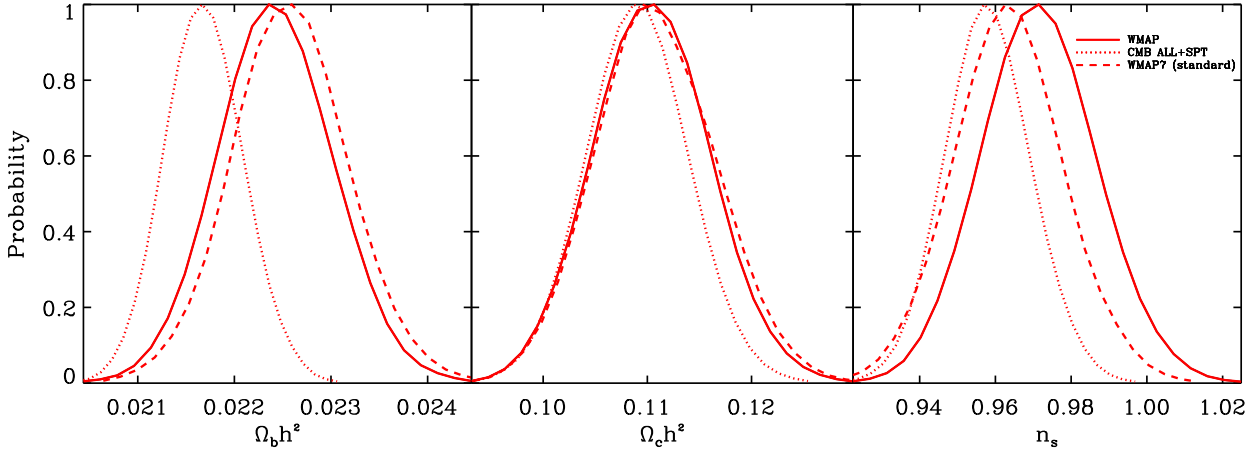


Figure 7. One dimensional posterior probability distribution of $\Omega_b h^2$, $\Omega_{\text{DM}} h^2$ and n_s parameters in the case of *WMAP7* dataset and no DM annihilation (dashed), *WMAP7* case (dotted) and *CMB ALL + SPT* case (dotted)

Table 2. 95% c.l. upper limit constraints on the DM annihilation cross-section $\langle\sigma v\rangle$ [10^{-26} cm³/s] in different cases of mass, annihilation channel and dataset considered.

Mass	WMAP7			CMB ALL+SPT		
	e^+e^-	$\mu^+\mu^-$	$\tau^+\tau^-$	e^+e^-	$\mu^+\mu^-$	$\tau^+\tau^-$
2 GeV	≤ 0.554	≤ 2.19	-	≤ 0.351	≤ 1.02	-
5 GeV	≤ 1.29	≤ 5.07	≤ 6.91	≤ 0.811	≤ 2.55	≤ 3.80
10 GeV	≤ 2.66	≤ 8.79	≤ 21.2	≤ 1.68	≤ 5.14	≤ 11.8
20 GeV	≤ 6.32	≤ 16.2	≤ 40.0	≤ 3.60	≤ 10.1	≤ 26.7

Parameter	WMAP7 (Standard)	WMAP7	CMB ALL+SPT
$\Omega_b h^2$	0.0226 ± 0.0006	0.0224 ± 0.0006	0.0217 ± 0.0004
$\Omega_{DM} h^2$	0.1109 ± 0.0056	0.1105 ± 0.0054	0.1099 ± 0.0049
θ_s	1.0388 ± 0.0027	1.0384 ± 0.0027	1.0397 ± 0.0015
τ	0.0884 ± 0.0152	0.0876 ± 0.0150	0.0831 ± 0.0138
n_s	0.9635 ± 0.0142	0.9716 ± 0.01479	0.9579 ± 0.0113
$\ln(10^{10} A_s)$	3.1904 ± 0.0457	3.1868 ± 0.0460	3.2122 ± 0.0446

Table 3. 68% c.l. constraints of the background cosmology parameters in the case of WMAP7 dataset with no DM annihilation (WMAP7 (standard)), compared with the WMAP7 case with DM annihilation, and the CMB ALL+SPT case.

by Galli et al. (2011): the difference originates from the inclusion of the low-energy processes inducing a net energy loss (i.e energy not going into heating, ionization or excitation). As explained in the Introduction, decreasing the energy deposition fractions makes the constraints weaker.

4 SUMMARY AND DISCUSSION

We have investigated the imprints left on the CMB temperature and polarization spectra by the energy deposition due to annihilations of one of the most promising DM candidate, a stable WIMP of mass $m_\chi = 1 - 20$ GeV annihilating into leptons. A major improvement with respect to previous similar studies is a detailed treatment of the annihilation cascade and its energy deposition in the cosmic gas. This is vital as this quantity is degenerate with $\langle\sigma v\rangle$.

We performed a Monte Carlo Markov Chain analysis using a modified version of the CosmoMC code and CMB data from the WMAP, QUaD and SPT experiments. By further marginalizing over the cosmological parameters of the background cosmology we obtain the constraints on the annihilation cross-section for each annihilation channel.

The strongest constraints are obtained by combining all the available datasets up to $\ell_{\max} = 3100$. If annihilation occurs via the $e^+ - e^-$ channel, a light WIMP can be excluded as a viable DM candidate in the above mass range. However, if annihilation occurs via $\mu^+ - \mu^-$ or $\tau^+ - \tau^-$ channels instead we find that WIMPs with $m_\chi > 5$ GeV cannot be ruled out at $2\text{-}\sigma$ c.l. to provide the cosmologically required DM content.

We have compared our results with the constraints obtained by assuming a simplified energy deposition model, as the one profusely used in the recent literature, and we found that realistic energy deposition descriptions can influence the resulting constraints up to 60%. A different analysis of the energy deposition uncertainties has been performed in Galli et al. (2012).

We expect that this approach will be relevant in particular with the upcoming Planck data, with its better sensitivity and which allow a better constraining of this additional sources of ionization.

ACKNOWLEDGMENTS

We thank C. L. Bianco for his precious help. We thank Silvia Galli, Fabio Iocco, Luca Maccione, Pasquale Dario

Serpico and Tracy Slatyer for useful comments and discussions. CE and SP acknowledge a Visiting Grant from SNS where part of this work has been carried out. CE acknowledges support from the Helmholtz Alliance for Astroparticle Physics funded by the Initiative and Networking Fund of the Helmholtz Association. The Dark Cosmology Centre is funded by the Danish National Research Foundation.

REFERENCES

- Aalseth C. E. et al., 2011a, Physical Review Letters, 106, 131301
- , 2011b, Physical Review Letters, 107, 141301
- Abdo A. A. et al., 2010, JCAP, 4, 14
- Ackermann M. et al., 2011, Physical Review Letters, 107, 241302
- Akerib D. S. et al., 2010, Phys. Rev. D, 82, 122004
- Anthony A. E., 2012, in American Astronomical Society Meeting Abstracts, Vol. 219, American Astronomical Society Meeting Abstracts 219, p. 212.04
- Aprile E. et al., 2011, Physical Review Letters, 107, 131302
- Baushev A. N., Federici S., Pohl M., 2012, Phys. Rev. D, 86, 063521
- Bernabei R. et al., 2008, European Physical Journal C, 56, 333
- , 2010, European Physical Journal C, 67, 39
- Bertone G., Silk J., 2010, Particle dark matter, Bertone G., ed., Cambridge University Press, p. 3
- Biermann P. L., Becker J. K., Caceres G., Meli A., Seo E.-S., Stanev T., 2010, ApJL, 710, L53
- Brown . M., et al., 2009, Astrophys.J., 705, 978
- CDMS II Collaboration et al., 2010, Science, 327, 1619
- Chen X., Kamionkowski M., 2004, Phys. Rev. D, 70, 043502
- Cholis I., Salucci P., 2012, Phys. Rev. D, 86, 023528
- Cirelli M., Iocco F., Panci P., 2009, JCAP, 10, 9
- Crocker R. M., Aharonian F., 2011, Physical Review Letters, 106, 101102
- Dobler G., Finkbeiner D. P., Cholis I., Slatyer T., Weiner N., 2010, ApJ, 717, 825
- Evoli C., Valdés M., Ferrara A., Yoshida N., 2012, MNRAS, 422, 420
- Finkbeiner D. P., 2004, arXiv:astro-ph/0409027
- Furlanetto S. R., Stoeve S. J., 2010, MNRAS, 404, 1869
- Galli S., Iocco F., Bertone G., Melchiorri A., 2009, Phys. Rev. D, 80, 023505
- , 2011, Phys. Rev. D, 84, 027302
- Galli S., Valdes M., Iocco F., Slatyer T., 2012, in preparation

- Giesen G., Lesgourgues J., Audren B., Ali-Haïmoud Y., 2012, arXiv:1209.0247
- Guo F., Mathews W. G., 2012, ApJ, 756, 181
- Hooper D., 2012, arXiv:1201.1303
- Hooper D., Finkbeiner D. P., Dobler G., 2007, Phys. Rev. D, 76, 083012
- Hooper D., Linden T., 2011a, Phys. Rev. D, 83, 083517
- , 2011b, Phys. Rev. D, 84, 123005
- Hütsi G., Chluba J., Hektor A., Raidal M., 2011, A&A, 535, A26
- Hütsi G., Hektor A., Raidal M., 2009, A&A, 505, 999
- Keisler R., Reichardt C., Aird K., Benson B., Bleem L., et al., 2011, Astrophys.J., 743, 28
- Komatsu E. et al., 2011, ApJS, 192, 18
- Larson D. et al., 2011, ApJS, 192, 16
- Lewis A., Bridle S., 2002, Phys. Rev. D, 66, 103511
- Lewis A., Challinor A., Lasenby A., 2000, Astrophys.J., 538, 473
- Mapelli M., Ferrara A., Pierpaoli E., 2006, MNRAS, 369, 1719
- Padmanabhan N., Finkbeiner D. P., 2005, Phys. Rev. D, 72, 023508
- Pandolfi S., Ferrara A., Choudhury T. R., Melchiorri A., Mitra S., 2011, Phys. Rev. D, 84, 123522
- Seager S., Sasselov D. D., Scott D., 1999, ApJL, 523, L1
- Shull J. M., 1979, ApJ, 234, 761
- Shull J. M., van Steenberg M. E., 1985, ApJ, 298, 268
- Slatyer T. R., Padmanabhan N., Finkbeiner D. P., 2009, Phys. Rev. D, 80, 043526
- Tauber J. A. et al., 2010, A&A, 520, A1
- Valdés M., Evoli C., Ferrara A., 2010, MNRAS, 404, 1569
- Valdés M., Ferrara A., Mapelli M., Ripamonti E., 2007, MNRAS, 377, 245
- van den Aarssen L. G., Bringmann T., Goedecke Y. C., 2012, Phys. Rev. D, 85, 123512
- Wong W. Y., Moss A., Scott D., 2008, MNRAS, 386, 1023
- XENON100 Collaboration et al., 2012, arXiv:1207.5988
- Zaldarriaga M. et al., 2008, arXiv:0811.3918

APPENDIX A: LOCAL DEPOSITION

We have assumed in this paper that photon energy deposition occurs locally, which is not true in general (see [Slatyer, Padmanabhan & Finkbeiner 2009](#)). In the following we show that this approximation is very accurate in the energy range of interest here. CMB photons gain energy as they are Inverse Compton scattered by energetic leptons. At each scattering event, a CMB photon with mean energy $E_{\gamma, \text{CMB}}$ will be upscattered to an energy equal to:

$$E_{\gamma} \approx \frac{4}{3} \gamma^2 E_{\gamma, \text{CMB}} = 0.73 \left(\frac{E_e}{\text{GeV}} \right)^2 \left(\frac{1+z}{600} \right) \text{ MeV} \quad (\text{A1})$$

where γ is the Lorentz factor for the lepton. At epochs in which energy deposition is important ($z \leq 1000$) such upscattered photons are subsequently mainly downgraded by Compton scattering with thermal electrons ([Chen & Kamionkowski 2004](#); [Slatyer, Padmanabhan & Finkbeiner 2009](#)).

To estimate the efficiency of this mechanism, we compare in Fig. A1 the Compton cooling time, $t_{\text{cool}}^{-1} = (d \ln E / dt) = c \sigma_T n_e (1+z)^3 \epsilon g(\epsilon)$, with the Hubble time,

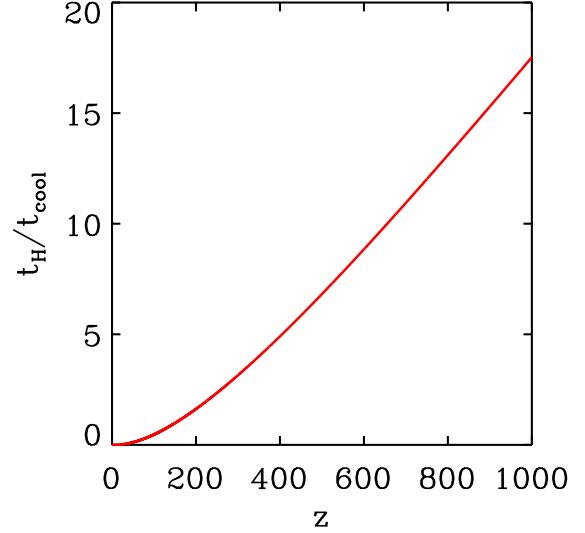


Figure A1. Ratio between Hubble time and Compton cooling time scales as function of the redshift.

$t_H = H^{-1}(z)$ where $\epsilon \equiv E_{\gamma}/m_e c^2$ and $g(\epsilon)$ is the classical Klein-Nishina cross-section. It is evident that the local deposition assumption, requiring $t_H \gg t_{\text{cool}}$, can be safely applied in the redshift range of interest here ($600 \lesssim z \lesssim 1000$)

APPENDIX B: FITTING FORMULAE

Below are the fitting formulae to the numerically derived energy depositions of electrons and positrons in the various channels.

$$f_h(x_e, z) = 10^{A(z)} (1 - C(z)(1 - x_e^{B(z)})) \quad (\text{B1})$$

$$f_{\text{ion}, H}(x_e, z) = 10^{A(z)} (1 - x_e^{B(z)})^{C(z)} \quad (\text{B2})$$

$$f_{\text{ion}, He}(x_e, z) = 10^{A(z)} (1 - x_e^{B(z)})^{C(z)} \quad (\text{B3})$$

where:

$$A(z) = A_0 + A_1 \log_{10} z + A_2 (\log_{10} z)^2 \quad (\text{B4})$$

$$B(z) = B_0 + B_1 \log_{10} z + B_2 (\log_{10} z)^2 \quad (\text{B5})$$

$$C(z) = C_0 + C_1 \log_{10} z + C_2 (\log_{10} z)^2 \quad (\text{B6})$$

The values of the parameters are given in Tab. B1.

Moreover we provide an updated version with respect to [Evoli et al. \(2012\)](#) for the energy deposition fractions that can be used for energies below the IC threshold: $E_{\text{th}} = ((1+z)/21)^{-1/2}$ MeV:

$$f_h(x_e) = a(1 - c(1 - x_e^b)) \quad (\text{B7})$$

$$f_{\text{ion}}(x_e) = a(1 - x_e^b)^c \quad (\text{B8})$$

where the values of the parameters are given in Tab. B2.

Table B1. Parameter values to be used in eq.s B1–B3

f_i	Channel	Mass	A_0	A_1	A_2	B_0	B_1	B_2	C_0	C_1	C_2
$f_{\text{ion,H}}$	$\mu^+\mu^-$	2	-1.996	1.668e-3	-1.049e-6	3.750e-1	-2.778e-5	-3.301e-8	9.643e-1	2.912e-5	-3.610e-7
$f_{\text{ion,H}}$	e^+e^-	2	-1.405	2.357e-3	-1.549e-6	3.820e-1	-1.612e-4	8.698e-8	1.014	-7.705e-4	3.240e-7
$f_{\text{ion,H}}$	$\mu^+\mu^-$	5	-1.937	2.538e-3	-1.664e-6	3.790e-1	-1.901e-4	1.225e-7	9.904e-1	-9.910e-4	6.400e-7
$f_{\text{ion,H}}$	e^+e^-	5	-1.678	3.279e-3	-2.211e-6	3.739e-1	-2.203e-4	1.744e-7	9.649e-1	-1.284e-3	1.038e-6
$f_{\text{ion,H}}$	$\tau^+\tau^-$	5	-1.853	1.758e-3	-1.093e-6	3.732e-1	-7.861e-5	2.318e-8	9.549e-1	-3.364e-4	4.671e-8
$f_{\text{ion,H}}$	$\mu^+\mu^-$	10	-2.053	2.927e-3	-1.944e-6	3.704e-1	-1.873e-4	1.408e-7	9.551e-1	-1.064e-3	8.178e-7
$f_{\text{ion,H}}$	e^+e^-	10	-1.888	3.890e-3	-2.648e-6	3.673e-1	-1.465e-4	1.159e-7	8.935e-1	-8.101e-4	7.575e-7
$f_{\text{ion,H}}$	$\tau^+\tau^-$	10	-2.117	1.975e-3	-1.245e-6	3.709e-1	-9.739e-5	4.789e-8	9.459e-1	-4.860e-4	2.286e-7
$f_{\text{ion,H}}$	$\mu^+\mu^-$	20	-2.256	3.536e-3	-2.383e-6	3.618e-1	-1.410e-4	1.246e-7	8.983e-1	-8.122e-4	7.281e-7
$f_{\text{ion,H}}$	e^+e^-	20	-2.100	4.393e-3	-2.980e-6	3.784e-1	-4.212e-5	-1.377e-8	8.560e-1	-3.335e-5	-3.348e-9
$f_{\text{ion,H}}$	$\tau^+\tau^-$	20	-2.317	2.608e-3	-1.699e-6	3.684e-1	-1.296e-4	9.050e-8	9.334e-1	-7.095e-4	5.067e-7
$f_{\text{ion,He}}$	$\mu^+\mu^-$	2	-2.521	9.046e-4	-3.260e-7	4.445e-1	1.200e-4	-1.484e-7	4.350e-1	1.148e-3	-1.260e-6
$f_{\text{ion,He}}$	e^+e^-	2	-1.978	1.916e-3	-1.026e-6	4.631e-1	-4.478e-5	1.766e-8	5.335e-1	2.848e-4	-5.717e-7
$f_{\text{ion,He}}$	$\mu^+\mu^-$	5	-2.514	2.391e-3	-1.445e-6	4.579e-1	-1.085e-4	6.551e-8	5.133e-1	-1.957e-4	-3.395e-8
$f_{\text{ion,He}}$	e^+e^-	5	-2.286	3.561e-3	-2.399e-6	4.558e-1	-1.212e-4	9.403e-8	5.343e-1	-6.910e-4	4.795e-7
$f_{\text{ion,He}}$	$\tau^+\tau^-$	5	-2.386	1.252e-3	-6.014e-7	4.441e-1	2.714e-5	-5.451e-8	4.389e-1	5.135e-4	-6.285e-7
$f_{\text{ion,He}}$	$\mu^+\mu^-$	10	-2.637	2.994e-3	-1.949e-6	4.444e-1	-1.203e-4	9.085e-8	4.894e-1	-4.346e-4	2.701e-7
$f_{\text{ion,He}}$	e^+e^-	10	-2.468	4.217e-3	-2.977e-6	4.687e-1	2.201e-5	-1.061e-7	5.021e-1	-4.570e-4	3.646e-7
$f_{\text{ion,He}}$	$\tau^+\tau^-$	10	-2.656	1.611e-3	-8.855e-7	4.410e-1	-5.718e-6	-1.931e-8	4.377e-1	2.615e-4	-3.665e-7
$f_{\text{ion,He}}$	$\mu^+\mu^-$	20	-2.830	3.732e-3	-2.569e-6	4.432e-1	-8.121e-5	7.030e-8	4.619e-1	-4.183e-4	3.644e-7
$f_{\text{ion,He}}$	e^+e^-	20	-2.634	4.431e-3	-3.097e-6	5.187e-1	-2.716e-4	1.468e-7	4.977e-1	-2.768e-4	2.312e-7
$f_{\text{ion,He}}$	$\tau^+\tau^-$	20	-2.872	2.494e-3	-1.573e-6	4.418e-1	-4.527e-5	2.369e-8	4.490e-1	-8.283e-5	-1.347e-8
f_h	$\mu^+\mu^-$	2	-1.621	1.851e-3	-1.269e-6	2.625e-1	1.347e-4	-1.029e-7	8.849e-1	-3.992e-5	1.456e-8
f_h	e^+e^-	2	-1.013	2.349e-3	-1.624e-6	2.670e-1	1.418e-4	-1.169e-7	8.860e-1	-8.014e-5	4.808e-8
f_h	$\mu^+\mu^-$	5	-1.546	2.419e-3	-1.606e-6	2.690e-1	1.011e-4	-8.034e-8	8.847e-1	-8.490e-5	6.019e-8
f_h	e^+e^-	5	-1.279	2.948e-3	-1.926e-6	2.794e-1	2.208e-5	-9.847e-9	8.807e-1	-9.096e-5	7.457e-8
f_h	$\tau^+\tau^-$	5	-1.476	1.828e-3	-1.197e-6	2.651e-1	1.146e-4	-8.667e-8	8.839e-1	-5.171e-5	2.939e-8
f_h	$\mu^+\mu^-$	10	-1.665	2.735e-3	-1.796e-6	2.734e-1	6.668e-5	-5.288e-8	8.815e-1	-8.244e-5	6.480e-8
f_h	e^+e^-	10	-1.516	3.609e-3	-2.362e-6	2.800e-1	-7.608e-5	8.341e-8	8.719e-1	-5.938e-6	3.950e-9
f_h	$\tau^+\tau^-$	10	-1.739	1.989e-3	-1.290e-6	2.668e-1	1.019e-4	-7.745e-8	8.830e-1	-5.687e-5	3.657e-8
f_h	$\mu^+\mu^-$	20	-1.881	3.307e-3	-2.166e-6	2.765e-1	-1.291e-5	1.540e-8	8.763e-1	-4.793e-5	4.419e-8
f_h	e^+e^-	20	-1.767	4.314e-3	-2.857e-6	2.580e-1	-6.141e-5	1.013e-7	8.787e-1	1.085e-5	-2.599e-8
f_h	$\tau^+\tau^-$	20	-1.938	2.507e-3	-1.627e-6	2.703e-1	6.107e-5	-4.581e-8	8.812e-1	-6.110e-5	4.604e-8

Table B2. Parameter values to be used in eq.s B7–B8

f_i	a	b	c
f_h	9.77e-1	3.00e-1	9.00e-1
$f_{\text{ion,H}}$	3.55e-1	3.90e-1	1.11
$f_{\text{ion,He}}$	6.10e-2	5.30e-1	1.05